Plasma Physics and Controlled Fusion

PAPER • **OPEN ACCESS**

Time-helicity de-resonation (T-H) diagram for energy-selective mixing of charged particles during sawtooth crashes in tokamaks

To cite this article: A Bierwage *et al* 2024 *Plasma Phys. Control. Fusion* **66** 065012

OPEN ACCESS
IOP Publishing
Plasma Physics and Controlled Fusion
Plasma Phys. Control. Fusion **66** (2024) 065012 (10pp)
https://doi.org/10.1088/1361-6587/ad4057

Time-helicity de-resonation (T-H) diagram for energy-selective mixing of charged particles during sawtooth crashes in tokamaks

A Bierwage[1,2,*], Ph Lauber[3] and K Shinohara[4,2]

[1] National Institutes for Quantum Science and Technology (QST), Rokkasho Fusion Institute, Aomori, Japan
[2] QST, Naka Fusion Institute, Ibaraki, Japan
[3] Max-Planck-Institut für Plasmaphysik, Garching, Germany
[4] Department of Complexity Science and Engineering, The University of Tokyo, Kashiwa, Chiba, Japan

E-mail: bierwage.andreas@qst.go.jp

Received 15 November 2023, revised 25 March 2024
Accepted for publication 18 April 2024
Published 29 April 2024

Abstract
It was recently shown that there exists a narrow parameter window where benign sawtooth crashes cause only mixing of bulk plasma and slowed-down alpha particle 'ash', while leaving MeV-class fast alphas largely unperturbed (Bierwage *et al* 2022 *Nat. Commun.* **13** 3941). Here, we revisit the underlying physical picture and reframe it in a manner that may be suitable for systematic analyses of this phenomenon in modeling, simulation and experimental studies. In particular, we propose a graph that we call 'time-helicity de-resonation diagram' (short: T-H diagram) that captures the physical essence of energy-selectivity of sawtooth-particle interactions and visualizes it in a compact, intuitive way. Moreover, the regimes of good confinement and strong mixing during a sawtooth crash can be discerned via a single figure of merit: the T-H radius. The concept is introduced here on the basis of simulation results and would eventually benefit from further validation when applied to suitable empirical data.

Keywords: tokamak, fast ions, MHD instability, transport

1. Introduction

For an efficient operation of a fusion power plant using magnetic confinement, without too-frequent restarts, two conditions must be satisfied simultaneously:

- Fast fusion-born alphas must remain in the plasma core to heat the fuel;
- Slowed-down alphas must be transported out of the core to limit dilution.

While this conundrum remains largely unresolved to this day, ideas exist that may at least alleviate the problem. For instance, self-organization processes such as the sawtooth crash in configurations like those shown in figure 1 are known to limit the accumulation of impurities in the central plasma core, so it has been reckoned that these internal relaxations may also be utilized for ash control. In 1996, Kolesnichenko & Yakovenko predicted that a typical sawtooth crash causes mixing of

* Author to whom any correspondence should be addressed.

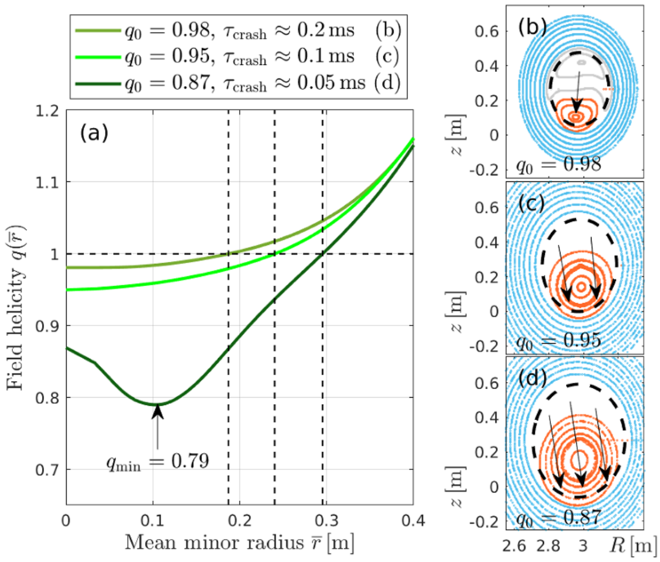

Figure 1. Three configurations for which sawtooth crashes and their influence on alpha particles were studied numerically in [9] and which we revisit here. Panel (a) shows the initial profiles of the safety factor q ($=$ magnetic field helicity). For each case, one snapshot of the magnetic field topology during the simulated sawtooth crash is shown in (b)–(d). Unreconnected flux surfaces with $q < 1$ and $q > 1$ are colored red and blue, respectively. Contours of reconnected flux ($=$ magnetic island) are colored gray in (b). The initial $q = 1$ surfaces are indicated by dashed lines, and the motion of the kinked core is indicated by arrows. Adapted from Supplementary figures 2, 5, 10 and 11 of [9], where much more detail can be found.

particles only below a certain critical energy [1]. Their prediction was confirmed by experiments and simulations; e.g. [2, 3]. However, the quality of energy selectivity was not sufficient in the cases that had been analyzed: although the density profile of slowed-down alpha ash was flattened reliably, the majority of fast alphas also suffered from strong mixing. It seemed that only trapped particles could effectively decouple from the reconnecting internal kink-interchange mode during a sawtooth crash, while passing particles would undergo mixing.

Recently, we revisited this problem by performing simulations with the MHD-PIC hybrid code MEGA [4, 5] for a configuration based on sawtoothing JET deuterium plasmas with major radius $R_0 = 3$ m, field strength $B_0 = 3.7$ T and plasma current $I_{\rm p} = 2.5$ MA [6, 7]. When the central safety factor was chosen to be close to unity ($q_0 \sim 1$), it was found that fusion-born alpha particles can maintain a peaked profile at high energies, while undergoing radial mixing at low energies as shown in figures 2(a)–(c) for the case with $q_0 = 0.98$ in the upper part of figure 1. In our simulations, the alphas were represented by passive tracer particles, so that they did not affect the kink dynamics. In this way, we eliminated numerical noise problems, effects of other resonantly driven Alfvén modes, and free (or unknown) parameters such as fusion reactivity and alpha particle concentration. This allowed us to focus on a well-defined and well-posed physics problem and close gaps in our understanding. The simulations were initialized with mono-energetic, nearly isotropic alpha distributions [8]. The key results were published in [9], whose appendices contain additional sensitivity tests and parameter scans.

In the present paper, we briefly review the results of that study and—following the request of some readers of [9]—provide a more compact depiction of the relevant physics. In particular, the synergy of four physical factors described in figure 6 of [9] is reduced to a description in terms of two parameters, H and T, each of which measures one aspect of resonance detuning as will be described in detail in section 2:

1. helicity detuning H: resonance shift;
2. temporal detuning T: phase averaging.

In a nutshell: Both parameters H and T incorporate the sensitivity of the kink-mode-particle interaction with respect to the proximity of the safety factor q to unity in the mixing region. This condition $q \sim 1$, in turn, enhances the sensitivity of the resonance with respect to the magnetic (∇B) drift, and the resulting resonance shift will be measured here by H. The magnetic drift also has some influence on the relative rate of phase averaging that will be measured by T.

This reduction to two parameters allows us to conveniently visualize the degree of energy-selectivity of a sawtooth crash in diagrammatic form, an example of which is shown in figure 2(d), which we will discuss in detail below. Based on this 'time-helicity de-resonation diagram' (short: T-H diagram), we then show how the criterion for energy-selective confinement or mixing can be compactly expressed in terms of a single figure of merit: the T-H radius.

As a brief side note: The word 'de-resonation' (adapted from complex vocal acoustic phenomena) was chosen to underline the fact that the process is considered to be more complex than mere resonance detuning. The rapidity of a sawtooth crash means that the magnetic configuration and electric field patterns evolve while the particles circulate around the torus and drift across the magnetic surfaces of the reconnecting system. Moreover, in sufficiently high concentration, the alpha particles may act back on the sawtooth crash dynamics—an effect that was ignored in the simulations on which the present work is based.

The present paper is meant to assist readers who intend to apply the findings of [9] in their research. We will thus assume that the reader is familiar with the contents of [9] and its supplementary material. Nevertheless, most of the references to [9] that appear in the text below are only meant to indicate where related information can be found if needed. For the most part, it should be possible to simply continue reading without following each cross-reference. This paper concludes with a discussion concerning possible extensions and limitations of the proposed recipe.

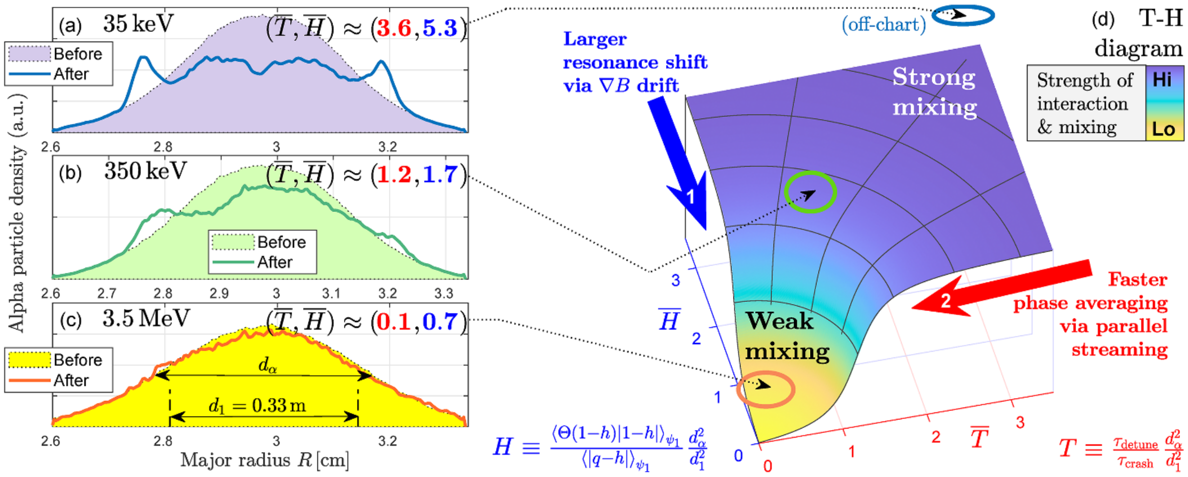

Figure 2. Density profiles of (a) alpha ash (35 keV), (b) intermediate (350 keV), and (c) fast alphas (3.5 MeV) before and after a sawtooth crash in a simulation with initial on-axis safety factor $q_0 = 0.98$ and sawtooth crash time $\tau_{\rm crash} \sim 0.2$ ms (adapted from figure 4 of [9]). The diameter $d_1 = 0.33$ m of the $q = 1$ surface and the half width d_α of the alpha density peak are indicated by double arrows in (c). The locations of the data points associated with panels (a)–(c) are indicated by open circles in panel (d), which shows the 'time-helicity de-resonation diagram' (short: T-H diagram). In this paper, we propose this T-H diagram as a compact way to visualize the physical principles that facilitate energy-selective confinement of particles during a sawtooth crash. Our model focuses on passing particles, which constitute the majority of the populations whose profiles are plotted in (a)–(c). The vertical scale for 'strength of interaction & mixing' in panel (d) is arbitrary. It was plotted here for schematic illustration using a simple hyperbolic tangent function with the point of inflection and nearby slope chosen to be roughly aligned with the observations made in our simulations. The parameters H and T are defined in equations (5) and (14), and values plotted in (d) are averages over co- and counter-passing particles, $\overline{H}$ and $\overline{T}$, as defined in equations (9) and (15). The data used to compute their values can be found in table 1.

2. Physics of energy-selectivity revisited

The results that are reproduced and analyzed in figure 2 belong to a case whose central safety factor q has been initialized with an on-axis value very close to unity: $q_0 = 0.98$. The initial $q(X)$ profile along the major radial coordinate $X = R - R_0$ is plotted as a green solid line in figure 3(a). The $q = 1$ radii (dashed lines) were chosen to match experimentally observed sawtooth mixing radii (see supplementary note 1 in [9]. Due to magnetic drifts, the spatial location of the magnetic resonance $q = 1$ differs from the location of a kinetic resonance, which is given by the condition

$$h = \omega_{\rm tor}/\omega_{\rm pol} = 1. \tag{1}$$

h is the orbit helicity; i.e. the kinetic generalization of the safety factor q ($=$ magnetic field helicity). $\omega_{\rm tor}$ and $\omega_{\rm pol}$ are the toroidal and poloidal transit frequencies of a particle's guiding center drift orbit. For an introduction to the underlying concept of a 'single species helicity', see section 3.8 of [10]. For application examples involving external magnetic perturbations, see [11, 12]. As representative examples, we have plotted in figure 3 the $h(X)$ profiles of co- and counter-passing alphas with low (35 keV) and high (3.5 MeV) kinetic energy $K = M_\alpha v^2/2$. The radial and vertical shifts of the h profiles relative to q are due to magnetic drifts and the mirror force [9]. Just as q_0 denotes the safety factor at the magnetic axis, h_0 will denote the orbit helicity at the locus of the stagnation orbit; i.e. the 'orbit axis', which corresponds to the minimum of h in figure 3.

As was already mentioned in the introduction, the energy-selective mixing of 35 keV alpha ash in figure 2(a) and robust peaking of newly-born 3.5 MeV alphas in figure 2(c) can be explained in terms of two factors, which are indicated by the large arrows in figure 2(d): 1. drift-induced resonant shift measured by H (blue), and 2. the amount of phase averaging during the sawtooth crash time $\tau_{\rm crash}$ measured by T (red). Both factors are influenced by magnetic drifts, whose strength can be measured by the difference $q - h$, and together with the mode amplitude they determine the strength of a particle's resonant interaction with the transient internal kink, whose domain extends here from the instantaneous reconnection layer (where $q = 1$) to the magnetic axis at $(X, Y) \equiv (R - R_0, z - z_0) = (0, 0)$.

The relative amount of mixing also depends (somewhat trivially) on the initial peakedness of the alpha particle density profile $n_\alpha(R)$ within the sawtooth mixing radius. Here, we measure this peakedness of $n_\alpha(R)$ by the parameter

$$D_{\rm peak} \equiv d_\alpha^2/d_1^2, \tag{2}$$

where d_α is the half-width of $n_\alpha(R)$ (i.e. its diameter measured at the height $\max\{n_\alpha\}/2$), and d_1 is the diameter of the $q = 1$ surface at the height of the plasma midplane ($Y \approx 0$). See the double arrows in figures 2(c) and 3. Both length scales appear squared in equation (2) to represent the respective area in the poloidal (R, z) plane. The inverse peak width parameter $D_{\rm peak}^{-1}$ is contained in both H and T of the T-H diagram in figure 2(d), which will be described in detail shortly. If the n_α profile is initially flat, so that $D_{\rm peak} \gg 1$, then H and T are reduced towards the domain of 'weak mixing' (or 'good confinement') by default. If the n_α profile is very sharply peaked, so that

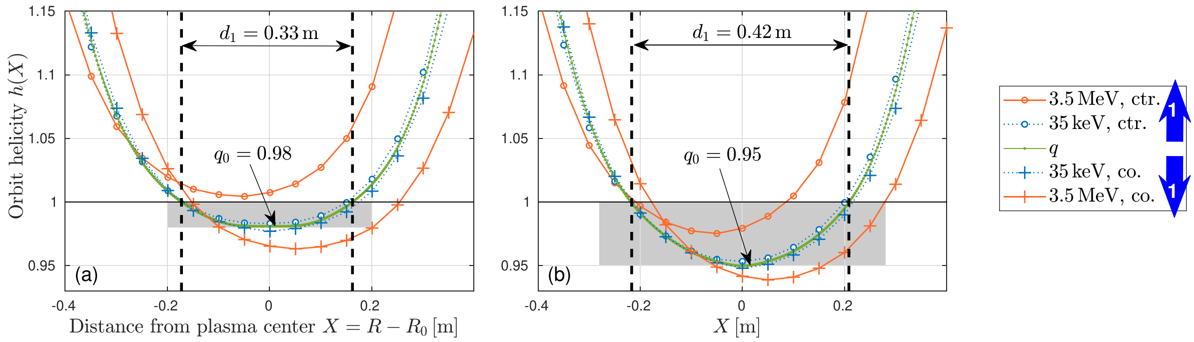

Figure 3. Orbit helicity profiles $h(X)$ (symbols), $q = 1$ radii (vertical dashed lines), and the approximate domain subject to reconnection (gray area) for our working examples with (a) $q_0 = 0.98$ and (b) $q_0 = 0.95$. Adapted from figure 7 and Supplementary figure 10 of [9]. Orbit helicity profiles $h(X)$ are plotted for fast alphas (3.5 MeV, orange) and helium ash (35 keV, light blue), and for both co-passing (co., $+$) and counter-passing (ctr., circles) particles. The safety factor profile $q(X)$ (solid green) lies between the curves $h[35\,\text{keV, co.}]$ and $h[35\,\text{keV, ctr.}]$. With increasing particle energy, the orbit helicity h increasingly departs from the safety factor q due to the increasing influence of magnetic (∇B) drifts, which is one of two necessary factors for particles to decouple from the kink mode. This trend is indicated by the blue arrows in the legend and corresponds to a decreasing value of the parameter H in figure 2(d) and equation (5), which measures the efficiency of helicity detuning via magnetic-drift-induced resonance shifts.

$D_{\rm peak} \ll 1$, then this profile is very likely to be broadened during the sawtooth crash, and this trend is represented by large values of H and T in the domain of 'strong mixing'.

Less trivial but well-known at least by experts in the field is the fact that fast ions detune from the kink more quickly than slow ions like alpha ash. This was illustrated in figures 6(d)–(f) of [9] and corresponds to the direction of the red arrow in figure 2(d). Energy-selective confinement is then possible if the sawtooth crash time is 'optimal' in the sense that

$$\tau_{\rm detune}(\text{fast}) < \tau_{\rm crash} < \tau_{\rm detune}(\text{ash}) \tag{3}$$

along the red T-axis in figure 2(d), where $T \propto \tau_{\rm detune}/\tau_{\rm crash}$ measures the efficiency of temporal detuning. This has been known at least since the seminal work by Kolesnichenko & Yakovenko [1], but it is only a necessary condition, not a sufficient one. In order to avoid the mixing of passing fast alphas, the above-mentioned sensitivity to magnetic drifts, facilitated by $q_0 \approx 1$, is also essential [9].

In the following, we describe our present recipe for constructing the parameters H and T, using simulation results from [9] as working examples. We focus on passing alphas since they constitute the majority of the population and because trapped particles tend to be generally less responsive to a sawtooth crash than passing ones.

2.1. Factor 1: Resonance shift via magnetic drifts (helicity detuning)

Electrons and slow ions have drift orbit surfaces (canonical toroidal angular momentum $P_\varphi = \text{const.}$) very close to magnetic flux surfaces ($\psi = \text{const.}$). Hence, their orbit helicity profiles satisfy $h \approx q$ and their resonances coincide roughly with $q = 1$ surfaces as the blue curves in figure 3 show for 35 keV alpha ash. In contrast, particles with large drifts have $h \neq q$ as the orange curves in figure 3 show for 3.5 MeV fast alphas. For q_0 sufficiently close to 1 as in figure 3(a), the location of the $h = 1$ resonant surfaces and their very existence then depends on the particle's energy and pitch[5].

The pitch-dependence implies that co- and counter-passing particles decouple from the kink in different ways. In the JET-based configuration that we have simulated in [9], the h profile of counter-passing 3.5 MeV alphas is raised above unity ($h_0 > 1$) when $q_0 \gtrsim 0.98$, so that there is no resonance at all as can be seen in figure 3(a). Their orbits undergo largely reversible distortions without topological change ('reconnection')[6]. Meanwhile, co-passing alphas have $h_0 < q_0$, so a resonance exists, but a large portion of it is located outside the $q = 1$ radius, where the internal kink has a small amplitude. In either case, the interaction and mixing are weak.

In summary, for both co- and counter-passing particles, the strength of magnetic drifts can be measured by the quantity $|q - h|$ and the proximity to the resonance can be measured by $|1 - h|$. The (pitch-dependent) existence condition of a resonance can be captured by the Heaviside step function

$$\Theta(1-h) = \begin{cases} 1 & : \quad h < 1, \\ 0 & : \quad \text{otherwise.} \end{cases} \tag{4}$$

From the above three factors, together with the inverse peak width parameter $D_{\rm peak}^{-1} \equiv d_1^2/d_\alpha^2$ from equation (2), we have constructed the following parameter H that measures the influence of drift-induced resonance shift, or helicity detuning:

$$H \equiv \frac{\langle \Theta(1-h)\,|1-h| \rangle_{\psi_{01}}}{\langle |q-h| \rangle_{\psi_{01}}} \frac{d_1^2}{d_\alpha^2}. \tag{5}$$

The brackets are flux-space-averages between the high-field-side (hfs) and low-field-side (lfs) $q = 1$ radii:

[5] The pitch-dependence in the case with $q_0 = 0.98$ was analyzed numerically in supplementary figure 8 accompanying [9].

[6] See supplementary figure 5 of [9].

$$\langle g \rangle_{\psi_{01}} \equiv \frac{1}{2\psi_1}\left(\int_0^{\psi_1} \mathrm{d}\psi\, g_{\mathrm{hfs}}(\psi) + \int_0^{\psi_1} \mathrm{d}\psi\, g_{\mathrm{lfs}}(\psi)\right), \quad (6)$$

where $\psi \in [0,1]$ is the normalized poloidal flux, and ψ_1 identifies the $q(\psi_1) = 1$ surface. $g(X)$ is an arbitrary integrable function defined on the midplane ($Y \approx 0$), and we write $g_{\mathrm{hfs}}(\psi) \equiv g(X \leqslant 0)$ and $g_{\mathrm{lfs}}(\psi) \equiv g(X \geqslant 0)$. (We chose to integrate over flux ψ based on the assumption that the intrinsic phase space density f_{eq} of a plasma in equilibrium satisfies $\partial f_{\mathrm{eq}}/\partial\psi = 0$; see [13].)

For quick estimates that do not require integration as equation (5), one may also try the simpler algebraic formula[7]

$$H^* \equiv \Theta(1-h^*)\frac{|1-h^*|}{|q_0 - h_0|}\frac{d_1^2}{d_\alpha^2}, \quad (7)$$

where the terms on the right-hand side are all initial (pre-crash) values, and where

$$h^* \equiv h_0 + \frac{1-q_0}{2}, \quad (8)$$

giving $1-h^* = 1-h_0-\frac{1}{2}(1-q_0) = \frac{1}{2}(1-h_0)+\frac{1}{2}(q_0-h_0)$, is an attempt to account for the q profile's temporal evolution[8] via the intermediate value $(1-q_0)/2$, located half-way between q_0 and 1. Meanwhile, $|q_0-h_0|$ is assumed to remain constant during the crash.

Tables 1 and 2 summarize the parameter values and results for the three cases from figure 1 with different q profiles (non-monotonic in table 2) and different crash times τ_{crash}. The values for co- and counter-passing alphas differ, so one may treat them separately or compute an average like

$$\overline{H} \equiv (H_{\mathrm{co}} + H_{\mathrm{ctr}})/2. \quad (9)$$

Efficient helicity detuning along the blue axis in figure 2(d) then corresponds to

$$H \lesssim 1 \quad \text{or} \quad \overline{H} \lesssim 1. \quad (10)$$

2.2. Factor 2: phase averaging via rapid parallel streaming (temporal detuning)

When $q \sim 1$ such that $h \sim 1$, many toroidal turns with period $\tau_{\mathrm{tor}} = 2\pi/\omega_{\mathrm{tor}}$ are needed for a particle's trajectory to fully cover a toroidal surface (in a manner similar to the apsidal precession in celestial mechanics) and to phase-average over the kink's mode structure. In [9], we have loosely defined the detuning time in the manner of an apsidal precession period,

$$\tau_{2\pi} \sim \tau_{\mathrm{tor}}/|1-h|, \quad (11)$$

which satisfies $\tau_{2\pi} \gg \tau_{\mathrm{tor}}$ in cases where $h \sim 1$. While equation (11) was sufficient for discussing the basic physical principles in [9] and for measuring the detuning time for a specific guiding center orbit in a given magnetic configuration, it can be useful to define a characteristic detuning time for sets of alpha particles with a certain kinetic energy K, like those in panels (a)–(c) of figure 2. One straightforward way to do so is to apply the integral in equation (6) to the denominator of equation (11) and define the effective detuning time

$$\tau_{\mathrm{detune}} \equiv \frac{\tau_{\mathrm{tor}}}{2\langle|1-h|\rangle_{\psi_{01}}}. \quad (12)$$

Notice that we included a factor 1/2 because temporal detuning starts to become effective for some particles when they are able to complete half a turn of apsidal precession during the crash time τ_{crash}: if a group of particles is initially convected radially outward by the kink's flow field, half an apsidal turn around the plasma center will bring it into a position, where the kink flow takes it back towards the center, thereby reversing the original displacement. By the same token, a full turn can be counter-productive. Many turns provide the most robust and comprehensive temporal detuning that is independent of initial positions.

For quick estimates, one may ignore the velocity-dependent magnetic drift effect in the detuning time and use the zero-orbit-width (ZOW) limit of equation (12),

$$\tau^*_{\mathrm{detune}} \equiv \frac{\tau_{\mathrm{tor}}}{2\langle|1-q|\rangle_{\psi_{01}}} \approx \frac{\tau_{\mathrm{tor}}}{|1-q_0|} \quad \text{(ZOW)}, \quad (13)$$

where we replaced h by q. For q profiles that are approximately parabolic in minor radius and, thus, linear in ψ, the integral can also be avoided and one obtains the simple algebraic formula on the right-hand side of equation (13).

Taking the ratio of the detuning time and the sawtooth crash time, and applying the inverse peaking factor $D_{\mathrm{peak}}^{-1} \equiv d_1^2/d_\alpha^2$ of equation (2), we have constructed the following parameter T that measures the influence of phase averaging, or temporal detuning:

$$T \equiv \frac{\tau_{\mathrm{detune}}}{\tau_{\mathrm{crash}}}\frac{d_1^2}{d_\alpha^2} = \frac{\tau_{\mathrm{tor}}}{\tau_{\mathrm{crash}}}\frac{d_1^2/d_\alpha^2}{2\langle|1-h|\rangle_{\psi_{01}}}. \quad (14)$$

The values for co- and counter-passing alphas differ, so one may treat them separately or compute an average,

$$\overline{T} \equiv (T_{\mathrm{co}} + T_{\mathrm{ctr}})/2. \quad (15)$$

Efficient temporal detuning along the red axis in figure 2(d) then corresponds to

$$T \lesssim 1 \quad \text{or} \quad \overline{T} \lesssim 1. \quad (16)$$

The presence of h in equations (12) and (14) implies that our convenient distinction between 'temporal detuning' and 'helicity detuning' is somewhat idealized and should not be read too literally. T is not entirely independent of H, and the detuning time is affected by magnetic drifts, as was already evident from its original form in equation (11) that we used in

[7] In cases with non-monotonic q profiles, q_0 and h_0 in equations (7) and (8) may have to be replaced by other suitable quantities to produce meaningful results. We have not done this yet, so no result for H^* are shown in table 2.

[8] See supplementary figure 9 of [9].

Table 1. Overview of detuning parameters $\overline{T}$ and $\overline{H}$ that we use to draw T-H diagrams like that in figure 2(d), and to compute the T-H radius $R_{\overline{TH}}$ as a single figure of merit for energy-selective particle confinement during a sawtooth crash. The table shows all factors that were used in the calculation of these parameters for alpha particles with kinetic energies $K = 35$, 350, 3500 keV in two cases that were studied in [9] and whose key parameters are shown in the top row. The respective q profiles are shown in figure 1(a). For all quantities that involve h, we distinguish between co- and counter-passing orbits, and the values for the latter are enclosed in parentheses. The toroidal transit period for $q \approx 1$ is computed as $\tau_{\rm tor} \approx 2\pi R_0/v$ with $R_0 = 3$ m and $v^2 = 2K/M_\alpha$, where $M_\alpha \approx 4M_{\rm p}$ is the approximate alpha particle mass. The drift parameter $q - h$ and the resonance distance $1 - h$ are obtained from h profiles like those in figure 3 (in [9], see figure 7 and supplementary figure 10). The evolution of the alpha particle density profiles in the case with $q_0 = 0.95$ can be found in Supplementary figure 13 of [9]. For the case with $q_0 = 0.98$, see figure 2 above.

Case:	$q_0 = 0.98$, $\tau_{\rm crash} = 0.2$ ms, co. (ctr.)			$q_0 = 0.95$, $\tau_{\rm crash} = 0.1$ ms, co. (ctr.)		
K (keV)	35	350	3500	35	350	3500
$\tau_{\rm tor}$ (μs)	15	4.6	1.5	15	4.6	1.5
(equation (2)) d_1 (m)/d_α [m]	0.33/0.33	0.33/0.34	0.33/0.38	0.42/0.33	0.42/0.34	0.42/0.38
$\langle \lvert 1-h \rvert \rangle_{\psi_{01}}$	0.0130	0.0168	0.0240	0.0277	0.0311	0.0378
	(0.0089)	(0.0064)	(0.0202)	(0.0239)	(0.0208)	(0.0246)
$\tau_{\rm detune}$ (ms)	0.58 (0.84)	0.13 (0.35)	0.031 (0.037)	0.27 (0.31)	0.072 (0.11)	0.020 (0.030)
(equation (14)) T	2.9 (4.2)	0.63 (1.7)	0.12 (0.14)	4.4 (5.1)	1.1 (1.7)	0.24 (0.37)
$\langle \lvert 1-q \rvert \rangle_{\psi_{01}}$	0.0111	0.0111	0.0111	0.0256	0.0256	0.0256
$\tau^*_{\rm detune}$ (ms)	0.68	0.20	0.068	0.29	0.088	0.029
(equation (17)) T^*	3.4	0.98	0.25	4.7	1.4	0.36
$\langle \lvert q-h \rvert \rangle_{\psi_{01}}$	0.0019	0.0057	0.0140	0.0022	0.0063	0.0188
	(0.0024)	(0.0077)	(0.0313)	(0.0022)	(0.0075)	(0.0347)
$\langle \Theta(1-h) \lvert 1-h \rvert \rangle_{\psi_{01}}$	0.0130	0.0168	0.0235	0.0277	0.0310	0.0356
	(0.0088)	(0.0049)	(0)	(0.0238)	(0.0196)	(0.0077)
(equation (5)) H	6.8 (3.7)	2.8 (0.60)	1.3 (0)	20.4 (17.5)	7.5 (4.0)	2.3 (0.27)
$q_0 - h_0$	0.0030	0.0081	0.0169	0.0021	0.0060	0.0112
	(−0.0032)	(−0.0090)	(−0.0244)	(−0.0033)	(−0.0093)	(−0.0252)
$1 - h_0$	0.0230	0.0281	0.0369	0.0521	0.0560	0.0612
	(0.0168)	(0.0110)	(−0.0044)	(0.0467)	(0.0407)	(0.0248)
(equation (8)) H^*	4.3 (2.1)	2.1 (0.10)	1.2 (0)	20.9 (10.7)	7.9 (2.6)	3.9 (0)
(equation (15)) $\overline{T}$	3.6	1.2	0.13	4.8	1.4	0.31
(equation (9)) $\overline{H}$	5.3	1.7	0.7	19.0	5.8	1.3
(equation (18)) $R_{\overline{\rm TH}}$	4.5	1.5	0.5	13.9	4.2	0.9

[9]. However, at least for the cases analyzed here, we find that the zero-orbit-width-limit

$$T^* \equiv \frac{\tau^*_{\rm detune}}{\tau_{\rm crash}} \frac{d_1^2}{d_\alpha^2} \quad \text{(ZOW)} \tag{17}$$

based on equation (13) yields values T^* that are often quite close to T, as one can verify in tables 1 and 2 for the three cases in figure 1.

3. The time-helicity de-resonation diagram (T-H diagram)

Resonance detuning in the time domain (captured by T) can also be realized by electrons due to their small mass and high speed, but they undergo strong mixing since their orbit surfaces change topology ('reconnect') in the same way as magnetic surfaces do. Only fast ions possess sufficiently high transit velocities (captured by T) and large magnetic drifts (primarily captured by H) to decouple from the crash dynamics, if the sawtooth crash is not too fast (see figure 8 of [9] for illustrative examples).

Apart from the trapped-passing boundary[9], there seems to be no sharp threshold for energy-selective confinement for a benign Kadomtsev-type sawtooth crash [14] followed by Wesson-type quasi-interchange flow [15] as we have considered here. Slower ions undergo stronger mixing than faster ones, and intermediate responses are obtained at intermediate energies as was shown in figure 2(a)–(c). The contour surface plot in figure 2(d) summarizes these principles and observations in compact form. Open circles in figure 2(d) indicate the data points for the three mono-energetic alpha particle populations in panels (a)–(c).

Here, 35 keV alpha ash is located around $(\overline{T}, \overline{H}) \approx (3.6, 5.3)$, off the upper right corner of the T-H diagram in figure 2(d). Newborn 3.5 MeV alphas occupy the lower left

[9] See supplementary figure 8 of [9].

Table 2. Same as table 1, but for the case with a non-monotonic q profile in figure 1(a) that has $q_0 = 0.87$ and $q_{\min} = 0.79$. For the h profiles and for the evolution of the alpha particle density profile, see supplementary figures 11 and 14 of [9].

Case: $q_{\min} = 0.79$, $\tau_{\rm crash} = 0.05\,$ms, co. (ctr.)			
$K\,$(keV)	35	350	3500
$\tau_{\rm tor}\,(\mu$s)	15	4.6	1.5
$d_1\,$(m)$/d_\alpha\,$[m]	0.53/0.33	0.53/0.34	0.53/0.38
$\langle\lvert 1-h\rvert\rangle_{\psi_{01}}$	0.1146 (0.1120)	0.1167 (0.1096)	0.1190 (0.1133)
$\tau_{\rm detune}\,$(ms)	0.066 (0.067)	0.019 (0.021)	0.0063 (0.066)
T	3.4 (3.5)	0.94 (1.00)	0.24 (0.26)
$\langle\lvert 1-q\rvert\rangle_{\psi_{01}}$	0.1131	0.1131	0.1131
$\tau^*_{\rm detune}\,$(ms)	0.066	0.020	0.0066
T^*	3.4	0.99	0.26
$\langle\lvert q-h\rvert\rangle_{\psi_{01}}$	0.0066 (0.0065)	0.0191 (0.0204)	0.0539 (0.0699)
$\langle\Theta(1-h)\times\lvert 1-h\rvert\rangle_{\psi_{01}}$	0.1145 (0.1119)	0.1162 (0.1082)	0.1134 (0.0943)
H	44.7 (44.4)	14.8 (12.9)	4.1 (2.6)
$\overline{T}$	3.5	0.97	0.25
$\overline{H}$	44.6	13.9	3.4
$R_{\overline{\rm TH}}$	31.6	9.9	2.4

corner around $(\overline{T},\overline{H}) \lesssim (0.1, 0.7)$, and intermediate 350 keV alphas are found near $(\overline{T},\overline{H}) = (1.2, 1.7)$ in the transition region between strong and weak mixing. Note that 10 keV electrons move about 5 times faster than newborn alphas and have Larmor radii $\rho_{\rm Le}$ about 50 times smaller than our alpha ash, so their coordinates have values on the order of $(T, H) \sim (0.02, 300)$, far outside the domain shown in figure 2(d). A logarithmic scale may be used if such data points were to be plotted. The obtained values for $\overline{T}$ and $\overline{H}$ in tables 1 and 2 are consistent with the simulation results in all cases inspected in terms of their location relative to the threshold for energy-selective confinement or, more accurately, the transition between strong and weak mixing.

While we have already invested some effort into defining T and H in a quantitatively meaningful manner, the form of the contours shown in our T-H diagram in figure 2(d)—a simple tanh function—serves only as a schematic illustration of the physical picture. With suitable refinements, this diagram may become a useful tool for quantitative predictions or modelling of energy-selective confinement. Discussions concerning trade-offs made between simplicity and accuracy can be found in section 5 below.

4. T-H radius: a single figure of merit for energy-selective confinement or mixing

The form of the contours in figure 2(d) reflects the fact that T and H represent two conditions that are both necessary but not sufficient on their own and must be satisfied simultaneously. One can reduce this diagram to a one-dimensional curve by defining a 'T-H radius'

$$R^2_{\overline{\rm TH}} \equiv \left(\overline{T}^2 + \overline{H}^2\right)/2, \tag{18}$$

where we used the averaged H and T parameters from equations (9) and (15), and the factor $1/2$ was chosen (somewhat arbitrarily) to give $R_{\overline{\rm TH}} = 1$ when $\overline{T} = \overline{H} = 1$. This allows one to express the criteria (10) and (16) for good confinement in compact form as

$$R_{\overline{\rm TH}} \lesssim 1 \quad \text{(weak mixing, good confinement).} \tag{19}$$

Tables 1 and 2 show the values for a few examples.

A single figure of merit such as $R_{\overline{\rm TH}}$ hides information about the dominant mechanism that controls the confinement of a given class or particles, so it is not as physically transparent as the underlying T-H diagram that, in turn, is based on the four physical ingredients described in figure 6 of [9]. However, $R_{\overline{TH}}$ in equation (18) may be more useful for practical modeling and computation tasks.

5. Summary and discussion

In [9], we and our collaborators advanced the theoretical understanding of fast ion confinement during sawtooth crashes by demonstrating the possibility of energy-selective mixing and confinement during such crashes and by clarifying the underlying physics. For reactor design, the requirement for large magnetic drifts (to shift or eliminate kink resonances when $q \sim 1$), means that small aspect ratio R/a and low current $I_{\rm p}$ are preferable if benign sawteeth are to be used for ash control; here, via radial mixing.

In the present paper, we devised the 'T-H diagram' in figure 2(d) for visualizing the physical requirements to realize both good confinement of fast alphas (needed for self-heating) and strong mixing of ash (to minimize fuel dilution). Based on the T-H diagram, the criterion for energy-selective confinement or mixing can be compactly expressed in terms of a single figure of merit, the 'T-H radius' in equation (18), as $R_{\overline{\rm TH}} \lesssim 1$. We hope that our condensed physical description in terms of 1. helicity detuning (H), and 2. temporal detuning (T), along with the proposed recipes for the construction of formulas for H and T, will make the findings of [9] more accessible for practical applications in the preparation and analysis of simulations and experiments.

It is important to keep in mind that the theoretical considerations made in [9] and here are based on the principle of separation of scales. The 'threshold' we are discussing here corresponds to the regime where scale separation vanishes; that is, where it switches between '$\gg 1$' and '$\ll 1$'. Consequently, the threshold $H \sim T \sim R_{\overline{TH}} \sim \mathcal{O}(1)$ is not sharp. It is only an order-of-magnitude estimate, so that the numerical value of the threshold may be somewhat smaller or larger than unity. In fact, the very definition of the 'threshold' is somewhat arbitrary: depending on the user's preferences, it may be placed at the top, center, or bottom of the transition. It is thus justified to apply customized scaling factors of order unity in the formulas (5) and (14) for H and T if needed.

Although the scale separation arguments on which our physical model is based are thought to provide a robust theoretical framework, the complexity of the dynamics cannot be fully captured. Hence, the quantitative predictions require further testing. Preferably, this should be done not only with numerical simulations but also real-world data, such as recent JET D-T experiments [16]. As was noted in [9], an experimental validation of our predictions and their practical utilization will require major advances in capabilities for core fueling, q profile measurements, and sawtooth crash control.

On the applied modeling side, there has been recent work on computationally efficient reduced fast ion transport models that took into account mechanisms responsible for energy- and pitch-selectivity of a sawtooth crash in order to improve the quantitative agreement with experimental measurements [17–22]. The methods proposed in the present paper may also be utilized in such efforts.

On the basic theory and simulation side, there are several avenues along which the methods proposed in this paper may be refined and generalized. For instance, one straightforward extension is to apply our equations to other rational surfaces $q = m_\psi/n$ and corresponding orbit resonances $h = m_{\rm orb}/n$, where n is the toroidal Fourier mode number and the integers m_ψ and $m_{\rm orb}$ identify the dominant poloidicity of the resonance on a magnetic flux surface or a drift orbit surface, respectively [23]. For instance, off-axis sawtooth crashes have been observed in the presence of multiple adjacent $q = 2$ surfaces, and one may look for energy-selectivity there. For such cases, the '1' appearing in equation (1) and in $1-h$ of equations (5) and (14) should be replaced by the appropriate value $h_{\rm res} \equiv m_{\rm orb}/n$ of the resonance considered:

$$H \equiv \frac{\langle \Theta\left(h_{\rm res} - h\right) |h_{\rm res} - h| \rangle_{\psi_{01}}}{\langle |q-h| \rangle_{\psi_{01}}} \frac{d_1^2}{d_\alpha^2} \tag{20a}$$

$$T \equiv = \frac{\tau_{\rm tor}}{\tau_{\rm crash}} \frac{1}{2\langle |h_{\rm res} - h| \rangle_{\psi_{01}}} \frac{d_1^2}{d_\alpha^2}. \tag{20b}$$

An important but significantly more difficult extension is the inclusion of the effect of mutual interactions between the plasma instabilities and alpha particles (here treated as passive test particles). In principle, their study is already possible with the hybrid code MEGA that we employed in [9]. However, we chose to postpone this task until we are able to properly account for the contribution of fast ions to the MHD equilibrium. Another extension to be considered is the inclusion of plasma rotation effects. Although rotation effects are expected to be relatively weak in the large burning plasmas of ITER and DEMO reactors to which the present work is primarily dedicated, plasma rotation is often important for low-frequency modes such as the internal kink in present-day externally heated plasmas. Plasma rotation may thus have to be included in validation studies, where our model could be tested against existing or near-term data. A thorough understanding of plasma rotation physics is required for this, which we do not currently have[10].

Of course, the intuitive appeal and utility of the T-H diagram in figure 2(c) relies on reasonable simplifications. As stated in the discussion section of [9]:'*[...] orbit helicity profiles also evolve in time, with a tendency to rise during the crash. Thus, the resonances are dynamic: their location, width and their very existence evolve rapidly. Moreover, the* $\boldsymbol{E}\times\boldsymbol{B}$ *flow pattern is nonuniform in space* [and evolves in time]. *Along particle orbits that perform large magnetic drifts, the direction of the electric drift may thus vary even during a single transit. This influences the effective magnitude of the electric drifts for fast alphas. Our simulations capture these complexities accurately, while also confirming the basic physical picture* [...].' Evidently, the transient, dynamic nature of a sawtooth crash makes the process of energy-selective confinement more complex than mere resonance *detuning*. As mentioned in the introduction, this is the reason why we chose the attribute *de-resonation* when naming the 'time-helicity (T-H) de-resonation diagram', whose basic concept was introduced here. It remains to be seen to what extent it will be possible to perform meaningful refinements without sacrificing the model's current merits. One valuable extension would be to construct a model that allows to quantify in a systematic manner the 'strength of interaction & mixing' that determines the shape of the surface contours in the T-H diagram, which we have drawn in figure 2(d) only in a schematic manner using a simple hyperbolic tangent function.

Finally, we note that the present (first) incarnation of the T-H diagram was devised for the analysis of energy-selective confinement in cases where transport is transient and dominated by $\boldsymbol{E}\times\boldsymbol{B}$ convection, such as a Kadomtsev-type sawtooth crash [14] and Wesson-type quasi-interchange [15]. Of course, energy- and pitch-selectivity due to magnetic drift effects in regions with relatively flat and near-resonant q profile arises also in association with transport that can occur in stationary or slowly evolving non-axisymmetric configurations, such as helically kinked cores and partially crashed sawtooth remnants (e.g. see [24–28]) or stellarators [29, 30]. It may be possible to find figures of merit like our T and H for such cases. For instance, T may be expressed in terms of coefficients that characterize transport in various forms. H may be written more explicitly in terms of the gyro- or drift-radius instead of our proxy parameter $q-h$, since h may not always be available (for instance, when kinetic chaos has developed).

[10] Merely adding a frequency shift in a resonance condition like equation (1) may not suffice to account for plasma rotation effects. For instance, one would have to evaluate the evolution of the pressure field and associated diamagnetic rotation in the kink's domain during the sawtooth crash. Further complications arise from the fact that the Doppler shifts of the bulk plasma and fast ions differ. Last but not least, radial electric fields that emerge when ions and electrons are transported at different rates should also be considered, but electron transport is still poorly understood. Neoclassical theory only partly captures the relevant physics and its experimental validation still seems to give mixed results.

Data availability statement

The data cannot be made publicly available upon publication due to legal restrictions preventing unrestricted public distribution. The data that support the findings of this study are available upon reasonable request from the authors.

Acknowledgments

This work builds on the results reported in [9], so we would like to express our gratitude to all co-authors of that study: Ye O Kazakov, V Kiptily, M Nocente, Ž Štancar, S Sumida, M Yagi, J Garcia, S Ide and JET Contributors. This work has been partly carried out within the framework of the EUROfusion Consortium, funded by the European Union via the Euratom Research and Training Programme (Grant Agreement No. 101052200—EUROfusion), within the framework of the Enabling Research Project 'ATEP'. Views and opinions expressed are however those of the authors only and do not necessarily reflect those of the European Union or the European Commission. Neither the European Union nor the European Commission can be held responsible for them.

ORCID iDs

A Bierwage https://orcid.org/0000-0003-1243-0502
K Shinohara https://orcid.org/0000-0003-1923-8441

References

[1] Kolesnichenko Y and Yakovenko Y 1996 Theory of fast ion transport during sawtooth crashes in tokamaks *Nucl. Fusion* **36** 159

[2] Muscatello C M, Heidbrink W W, Kolesnichenko Y I, Lutsenko V V, Van Zeeland M A and Yakovenko Y V 2012 Velocity-space studies of fast-ion transport at a sawtooth crash in neutral-beam heated plasmas *Plasma Phys. Control. Fusion* **54** 025006

[3] Jaulmes F, Westerhof E and de Blank H J 2014 Redistribution of fast ions during sawtooth reconnection *Nucl. Fusion* **54** 104013

[4] Todo Y and Sato T 1998 Linear and nonlinear particle-magnetohydrodynamic simulations of the toroidal Alfvén eigenmode *Phys. Plasmas* **5** 1321

[5] Todo Y, Shinohara K, Takechi M and Ishikawa M 2005 Nonlocal energetic particle mode in a JT-60U plasma *Phys. Plasmas* **12** 012503

[6] Nocente M *et al* 2020 Generation and observation of fast deuterium ions and fusion-born alpha particles in JET D–^{3}He plasmas with the 3-ion radio-frequency heating scenario *Nucl. Fusion* **60** 124006

[7] Kazakov Y O *et al* (JET Contributors, ASDEX Upgrade Team, EUROfusion MST1 Team and Alcator C-Mod Team) 2021 Physics and applications of three-ion ICRF scenarios for fusion research *Phys. Plasmas* **28** 020501

[8] Bierwage A, Fitzgerald M Lauber P, Salewski M, Kazakov Y and Štancar Ž 2022 Representation and modeling of charged particle distributions in tokamaks *Comput. Phys. Commun.* **275** 108305

[9] Bierwage A *et al* 2022 Energy-selective confinement of fusion-born alpha particles during internal relaxations in a tokamak plasma *Nat. Commun.* **13** 3941

[10] Bellan P M 2000 *Spheromaks: A Practical Application of Magnetohydrodynamic Dynamos and Plasma Self-Organization* (Imperial College Press)

[11] Shinohara K, Bierwage A, Suzuki Y, Kim J, Matsunaga G, Honda M and Rhee T 2018 Estimation of orbit island width from static magnetic island width, using safety factor and orbit pitch *Nucl. Fusion* **58** 082026

[12] Shinohara K, Bierwage A, Matsuyama A, Suzuki Y, Matsunaga G, Honda M, Sumida S and Kim J 2020 Efficient estimation of drift orbit island width for passing ions in a shaped tokamak plasma with a static magnetic perturbation *Nucl. Fusion* **60** 096032

[13] Hasegawa A, Chen L and Mauel M E 1990 A D-^{3}He fusion reactor based on a dipole magnetic field *Nucl. Fusion* **30** 2405

[14] Kadomtsev B B 1975 Disruptive instability in tokamaks *Sov. J. Plasma Phys.* **1** 389Plazmy F 1975 *Sov. J. Plasma Phys.* **1** 710–5

[15] Wesson J A 1986 Sawtooth oscillations *Plasma Phys. Control. Fusion* **25** 243

[16] Maggi C F (JET Contributors) 2023 Overview of T and D-T results in JET with ITER-like wall *Nucl. Fusion* (https://doi.org/10.1088/1741-4326/ad3e16) accepted

[17] Kim D, Podestà M, Liu D and Poli F M 2018 Orbit modeling of fast particle redistribution induced by sawtooth instability *Nucl. Fusion* **58** 082029

[18] Kim D, Podestà M, Liu D, Hao G and Poli F M 2019 Investigation of fast particle redistribution induced by sawtooth instability in NSTX-U *Nucl. Fusion* **59** 086007

[19] Teplukhina A A *et al* 2021 Fast ion transport by sawtooth instability in the presence of ICRF-NBI synergy in JET plasmas *Nucl. Fusion* **61** 116056

[20] Vallar M *et al* (the TCV Team) 2022 Modelling of sawtooth-induced fast ion transport in positive and negative triangularity in TCV *Nucl. Fusion* **62** 026028

[21] Podestà M, Gorelenkova M, Gorelenkov N N, White R B, Bonofiglo P J, Poli F M, Teplukhina A, Yang J, Cecconello M and Vallar M 2022 Development of a reduced model for energetic particle transport by sawteeth in tokamaks *Plasma Phys. Control. Fusion* **64** 025002

[22] Bonofiglo P J, Podestà M, Vallar M, Gorelenkov N N, Kiptily V, White R B, Giroud C and Brezinsek S (JET Contributors) 2022 Numerical studies on saturated kink and sawtooth induced fast ion transport in JET ITER-like plasmas *Nucl. Fusion* **62** 112002

[23] Bierwage A and Shinohara K 2014 Orbit-based analysis of resonant excitations of Alfvén waves in tokamaks *Phys. Plasmas* **21** 112116

[24] Farengo R, Ferrari H E, Firpo M-C, Garcia-Martinez P L and Lifschitz A F 2012 Alpha particle redistribution due to experimentally reconstructed internal kink modes *Plasma Phys. Control. Fusion* **54** 025007

[25] Farengo R, Ferrari H E, García-Martínez P L, Firpo M-C, Ettoumi W and Lifschitz A F 2013 Redistribution of high energy alpha particles due to sawteeth with partial reconnection *Nucl. Fusion* **S3** 043012

[26] Pfefferlé D, Graves J P, Cooper W A, Misev C, Chapman I T, Turnyanskiy M and Sangaroon S 2014 NBI fast ion confinement in the helical core of MAST hybrid-like plasmas *Nucl. Fusion* **54** 064020

[27] Pfefferlé D, Graves J P and Cooper W A 2015 Hybrid guiding-centre/full-orbit simulations in non-axisymmetric magnetic geometry exploiting general criterion for

guiding-centre accuracy *Plasma Phys. Control. Fusion* **57** 054017
[28] García-Martínez P L, Farengo R and Ferrari H E 2023 Energy dependent alpha particle redistribution in ITER like plasmas with a helical core *29th IAEA Fusion Energy Conf. (FEC 2023)* (*London, U.K. 16–21*)
[29] White R, Bierwage A and Ethier S 2022 Poor confinement in stellarators at high energy *Phys. Plasmas* **29** 052511
[30] Moseev D *et al* 2024 Influence of sawtooth oscillations on fast ions in a stellarator *Nucl. Fusion* (https://doi.org/10.1088/1741-4326/ad4169) accepted